University of São Paulo
"Luiz de Queiroz" College of Agriculture

Aerial machine vision, geographical information system and hue for pattern classification in agriculture

Marcel Pinton de Camargo

Dissertation presented to obtain the degree of Master in Science: Area: Agricultural Systems Engineering

Piracicaba
2018

Marcel Pinton de Camargo
Biosystems Engineering

Aerial machine vision, geographical information system and hue for pattern classification in agriculture

versão revisada de acordo com a resolução CoPGr 6018 de 2011

Advisor:
Profa. Dra. **TAMARA MARIA GOMES**

Dissertation presented to obtain the degree of Master in Science: Area: Agricultural Systems Engineering

Piracicaba
2018

Dados Internacionais de Catalogação na Publicação
DIVISÃO DE BIBLIOTECA – DIBD/ESALQ/USP

Camargo, Marcel Pinton de

Aerial machine vision, geographical information system and hue for pattern classification in agriculture / Marcel Pinton de Camargo. - - versão revisada de acordo com a resolução CoPGr 6018 de 2011. - Piracicaba, 2018.

41 p.

Dissertação (Mestrado) - - USP / Escola Superior de Agricultura “Luiz de Queiroz”.

1. Agricultura de precisão 2. Aerofotogametria 3. QGIS 4. Python 5. Reuso agrícola I. Título

SUMMARY

ACKNOWLEDGMENTS

This study was financed in part by the Coordenação de Aperfeiçoamento de Pessoal de Nível Superior - Brasil (CAPES) - Finance Code 001

RESUMO

Visão de máquina aérea, sistema de informação geográfica e matiz para classificação de padrões na agricultura

Nesta pesquisa pretendemos alcançar a coesão cibernética no fluxo de informações dentro da agricultura de precisão, integrando métodos de aprendizagem de máquinas, visão computacional, sistema de informação geográfica e aerofotogrametria em uma área irrigada com efluente de matadouro, sob cinco tratamentos (W100 - irrigação com água superficial e 100 % de adubação mineral nitrogenada, E0, E33, E66 e E100 - irrigação com efluente tratado de abatedouro e adição de 0, 33, 66 e 100% de adubação mineral nitrogenada, respectivamente) e quatro repetições em pastagem (Cynodon dactylon (L.) Pers.) Várias imagens (entre cem e duzentas) com modelo de cor vermelho, verde e azul (RGB) foram capturadas por um quadricóptero voando a 20 metros de altitude, e obtendo resolução espacial de 1 centímetro em uma superfície de aproximadamente 0.5 ha. As imagens foram ortorretificadas juntamente com nove pontos de controle, realizados pelo sistema de posicionamento global diferencial (GPS), ambos processados no software Agisoft PhotoScan. Treze projetos fotogramétricos foram realizados ao longo do tempo com revisita de 30 dias, a raiz do erro quadrático médio (RMSE) foi usada como medida de acurácia e atingiu valores menores que 5 centímetros para os eixos x, y e z. A ortoimagem obtida com a fotogrametria do veículo aéreo não tripulado (UAV) foi alterada de RGB para matiz, saturação, valor (HSV) e o espaço de cor matiz foi escolhido devido a independência da iluminação, além de ter boa descrição da exposição do solo e vegetação.Entretanto este é dependente da temperatura da fonte de luz, portanto difícil de se estabelecer um limiar estático, logo selecionamos um método de classificação não supervisionado, o K-Means, para classificar os padrões desconhecidos ao longo da área. Polígonos foram traçados delimitando a área representada por cada parcela e um método supervisionado de classificação baseado na entropia foi utilizado, a árvore de decisão, para explorar e encontrar padrões que reconheçam cada tratamento. Essas etapas também são exibidas em formas de mapas temáticos georeferenciados e foram executadas nos softwares de código aberto Python, QGIS e Weka. As regras definidas no espaço de cor matiz atingiram uma acurácia de 100% no conjunto de treinamento e proporcionaram um melhor entendimento sobre a distribuição do solo e da vegetação nas parcelas. Esta metodologia mostra um grande potencial para análise de dados na agricultura de precisão.

Palavras-chave: Agricultura de precisão; Aerofotogametria; QGIS; Python; Reuso agrícola

ABSTRACT

Aerial machine vision, geographical information system and hue for pattern classification in agriculture

In this research we aim to achieve cybernetic cohesion information flow in precision agriculture, integrating machine learning methods, computer vision, geographical information system and UAV-photogrammetry in an irrigated area with slaughterhouse wastewater, under five treatments (W100 - irrigation with superficial water and 100% of nitrogen mineral fertilization, E0, E33, E66 and E100 - irrigation with treated effluent from slaughterhouse and addition of 0, 33, 66 and 100% of nitrogen mineral fertilization, respectively) and four replications on grassland (Cynodon dactylon (L.) Pers.). Several images (between one hundred and two hundred) with red, green, blue (RGB) color model were captured using a quadcopter flying at 20 meter altitude and obtaining spatial resolution of 1 centimeter on a surface of approximately 0.5 ha. The images were orthorectified together with nine ground control points done by differential global positioning system (GPS), both processed in the Agisoft PhotoScan software. Thirteen photogrammetric projects were done over time with 30-day revisit, the root mean squared error (RMSE) was used as accuracy measurement, and reached values lower than 5 centimeters for x, y and z axis. The orthoimage obtained with unmanned aerial vehicle (UAV) photogrammetry was changed from RGB to hue, saturation, value (HSV) color model, and the hue color space was chosen due to independence of illumination, beyond it has a good description of exposure of soil and vegetation, but it is dependent of light source temperature, so difficult to estabilish a static threshold, so we selected an unsupervised classification method, K-Means, to classify the unknown patterns along the area. Polygons were drawn delimiting the area represented by each portion and a supervised classification method based on entropy was used, the decision tree, to explore and find patterns that recognize each treatment. These steps are also displayed in forms of georeferenced thematic maps and were executed in the open source softwares Python, QGIS and Weka. The rules defined on the hue color space reached an accuracy of 100% on the training set, and provided a better understanding about the distribution of soil and vegetation on the parcels. This methodology shows a great potential for analysis of spectral data in precision agriculture.

Keywords: Precision agriculture; UAV-photogrammetry; QGIS; Python; Agricultural reuse

1. INTRODUCTION

The integration between the computational intelligence and geographic information system reaches a degree of cybernetic cohesion in information flow worthy of third revolution in the area of computing and geographic quantification (Openshaw, 1992). The alliance of these areas has been successfully used recently to identify fire susceptibility in forests (Bui et al., 2017), locate suitable areas for water catchment in rivers (Al-Abadi et al., 2017), suggest favorable areas to rice cultivation (Maddahi et al., 2017), to map the risk of erosion in soils (Ai et al., 2013).

Emergent option in the area of remote sensing for the management of farms, are the remotely piloted aircraft with vertical take-off and landing, that counts on technological advances in the control and planning of autonomous flights (Duan *et al.*, 2017). The aerial imagery is able to provide the land planialymetry, essential information to help understanding the spatial variability of the crop and soils (Molin et al., 2015). Some demands in the area of remote sensing by remotely piloted aircraft are in the confidence of the final product, standardization of the georeferencing and mosaic of the images, flow for extraction of the information, advances in the design of the platforms (Zhang e Kovacs, 2012). The advantage of the information obtained by this aerial platform lies in the readiness of the image in raster data structure, where the pixels are the smallest informative elements and together of their neighbors form the grid matrix, with more than one attribute analyzed form the grid matrix with tessellated structure. This form of data organization facilitates the process of automation and implementation of computational algorithms (Burrough et al., 2015). In the geographical information system, the improvement in the accuracy of the latitude, longitude and height attributes is achieved with the use of modernized GPS that have the codes of the spectral signals L5 (1176.45 MHz), L2C (1227.60MHz) and L1C (1575.42MHz), broadly used in civil applications (Grewal et al., 2013).

Light is considered an electromagnetic radiation, produced by electrically charged particles, described in terms of wavelengths (Foley and Matlin, 2010), and comprises the visible region (400 to 700 nanometers) in electromagnetic spectrum. Because it encompasses considerable visible light, RGB (Red, Green, Blue) digital images are extensively used to extract information from agricultural crops (Molin et al., 2015). The RGB color space is extensively used by many schools around the world for machine vision systems, although its components are strongly correlated with lighting conditions, and therefore sensitive to these changes, especially in outdoor fields where conditions vary rapidly (Meng et al., 2015). Finally, the relationships between bands are unsuccessful attempts to eliminate the adverse effect of lighting (Liu and Moore, 1990).

An "intuitive" development of color spaces, designed in the way human perception is the HSV (Hue, Saturation, Value). In the transformation of the RGB-HSV color spaces, the data leave the Maxwell triangle and pass to the Cartesian coordinates (Meng et al., 2015). In this new arrangement there is the decoupling of luminance (V) and chromaticity (H + S). Hue provides the numerical description of the spectral range or dominant wavelength in a primary color mixture, so the problem of light dependence is avoided (Liu and Moore, 1990). However, changes in the temperature of the light source imply variations in the perceived hue of objects, so in open fields, it is little adherent to fix a threshold for segmentation or extraction of information in images (Ruiz-Ruiz et al., 2009).

The impasse of variable illumination condition for image acquisition in outdoor fields, is solved by using an automatic grouping method for machine learning, the K-means. This is a compact, powerful, unsupervised clustering algorithm for partitioning data sets into separate, predetermined groups. In histograms characterized by flat spaces with one dimension, the euclidean distance (sum of the quadratic errors), is the score function that must be minimized, the algorithm becomes a Hill-Climbing method, where at each interation the solution is improved and the sum of squared errors converge to a local minimum (Zaki and Meira, 2014). In practice the user predetermines the number of groups that the samples will be partitioned, the algorithm is executed multiple times and the best solution is chosen, assuming that it is a global minimum. In precision agriculture the use of k-means on the channel hue, with four and two clusters, results in the separation between soil and vegetation (Ruiz-Ruiz et al., 2009).

One need for precision agriculture is to identify heterogeneous areas to assert the concept of applications at variable rates. Another method of learning machine specialized in this topic are the decision trees. These were used for greenness identification (Yang *et al.*, 2015) and are constructed recursively from top to bottom, using divide and conquer algorithm, consisting of internal nodes representing the decisions corresponding to the division points, and the leaves representing the partitions in the data spaces in which the majority classes are designated (Silva *et al.,* 2010). There is a wide range of heuristics to choose the attribute, one much used is information gain, based on entropy. This measures the amount of disorder or uncertainty of a system, the division point that provides better discrimination between classes is one that has the highest information gain and greater reduction in entropy. A tree can be read as a set of decision rules, the set of rules can be interpreted as a set of alternatives or disjunctions, and cover the whole space, therefore can be transformed into a rules induction system (Zaki and Meira, 2014).

2. GERAL OBJECTIVE

Achieve cybernetic cohesion information flow by integration of unmanned aerial vehicle photogametry, computer vision techniques, machine learning algoritms, precision agriculture diferential global positioning system, that are able to extract nuances of a crop in timely and reliability manner.

2.1. Specifics objectives

To evaluate the time required for the construction of the georeferenced orthomosaic with channels red, green and blue.

To integrate the world wide known open source softwares, Quantum GIS, Python and Weka to interpret the information coming from the georeferenced orthomosaic.

To apply some of the wide range of available computer algorithms within the softwares used, which can be able to extract information from a crop in an area of agricultural reuse.

3. MATERIALS AND METHODS

3.1. Cybernetic Coesion Information Flow

In order to know the cybernetic coesion information flow from a cultivated field with an experimental crop about 200 images were used acquired via a digital format red, green, blue (RGB) camera coupled to an aerial platform. The exact location of each attribute was obtained with the use of control points, positioned with georreferencing of precision.

The images and control points were orthorectified by Agisoft PhotoScan Professional software. The main products were the RGB raster map and the terrain digital elevation model. With this methodology we explored the first product, the following steps were directed to compact, reduce and extract important information about the object of study. A great facility found in spectral information is the data fusion permissiveness, so it becomes feasible to use set theory.

A world-wide-used data analysis platform is the open-source software Python 2.7, in this release the OpenCV, Matplotlib and Numpy libraries are well implemented and are responsible for the computational vision, figure plots and scientific computing packages.

In the raster map the plots were manually delimited under visual examination of the RGB color channels, then this has undergone a transformation of the RGB color space to the hue, saturation, value (HSV), the hue channel was chosen. The histograms were normalized, and the K-means algorithm with 6 clusters was applied.

These steps gain greater visibility with geographic interpretation, so they were taken to the open source software world-wide used QGIS 2.18.13. This platform is a specialist within the geographic information system, so a wide range of additional tools to Python 2.7 is available, among them the generation of useful maps in planning, management and analysis of land suitability (Maddahi et al., 2017). For the success of this procedure it is essential to use control points with tiny errors.

Information on agricultural crops was exported in text format and delivered to other well-known open-source software, WEKA 3.8, which has many algorithms for data mining. In WEKA 3.8 the decision tree was performed and the reports on classifier evaluation, confusion matrices and rules were automatically issued (figure 1).

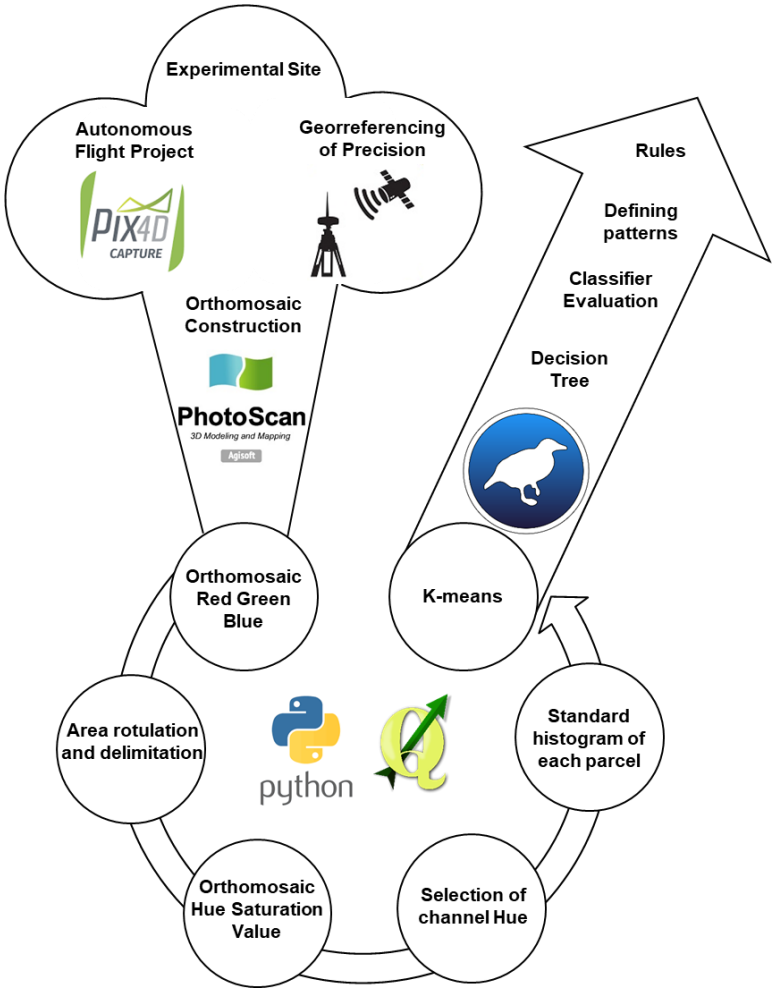

Figure 1. Cybernetic Cohesion Information Flow. Source: Own autor.

3.2. Experimental Site

The scientific experiment was located at the College of Animal Science and Food Engineering, University of São Paulo, Pirassununga/SP, Southeast Brazil. The experimental design was in random blocks, with four replications and five treatments as follows: (i) W100 - water irrigation with 100% of nitrogen mineral fertilization; E0, E33, E66 and E100 - irrigation with treated effluent from slaughterhouse and addition of 0, 33; 66 and 100% nitrogen mineral fertilization, respectively. Being the nitrogen fertilization (NF) 300 kg ha^{-1} $year^{-1}$ of nitrogen, in the form of urea. The crop cultivated is coastcross-grassland (Cynodon dactylon(L.)Pers.) planted in march 2012, the reactor UASB (upflow anaerobic sludge blanket) started the effluent treatment of wastewater slaughterhouse in April 2017, the sprinkler irrigation system was installed in October 2016 with irrigation interval of two days and the crop cuts occurred when reaching the height of 0.25 m.

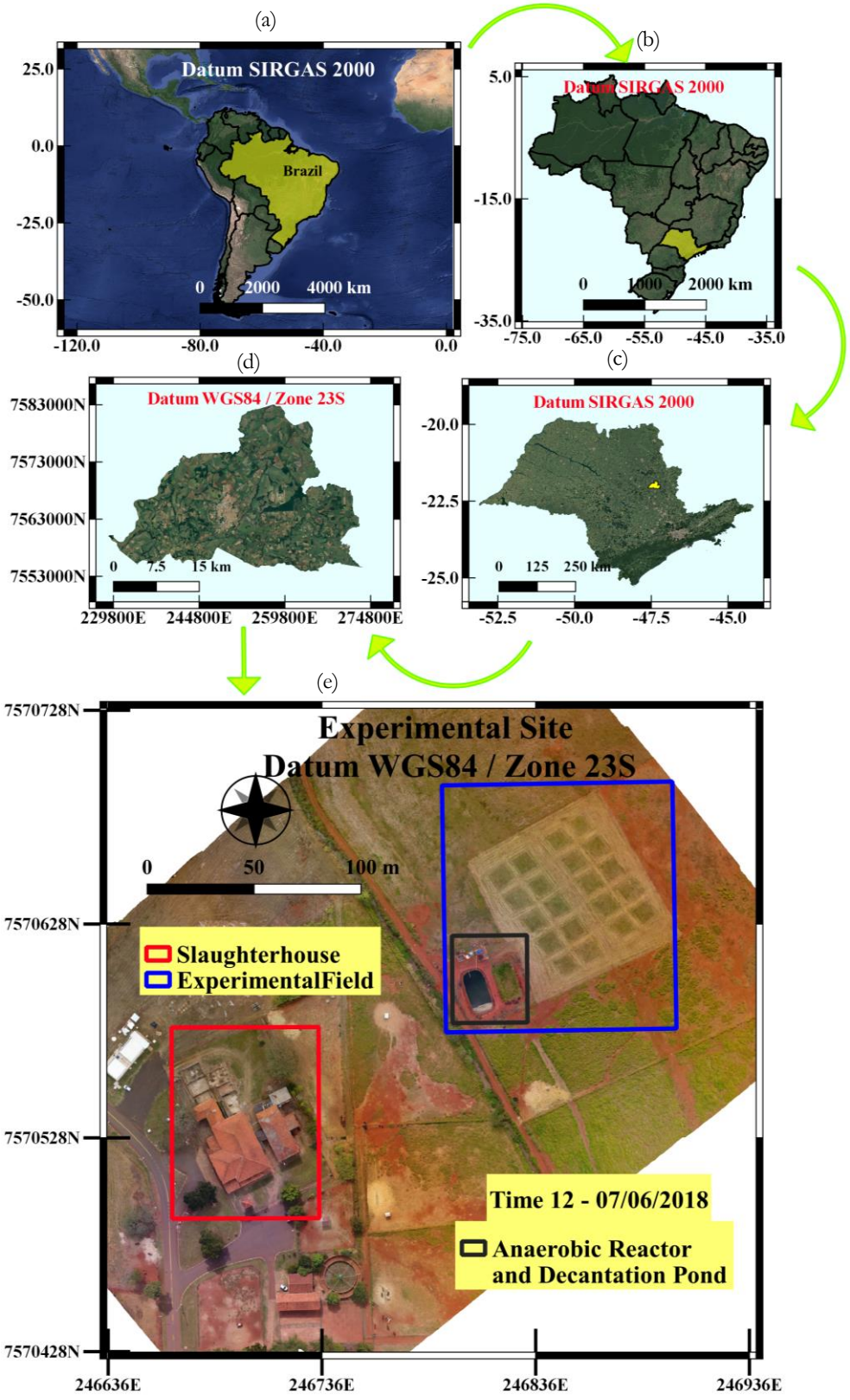

Figure 2. Aerial overview of (a) South America continent, (b) Brazilian country, (c) state of São Paulo, (d) city of Pirassununga and (e) experimental site located in College of Animal Science and Food Engineering, University of São Paulo. Source: Google Maps and own author.

3.3. Autonomous Flight Project

Phantom 4's remotely piloted aircraft from Chinese company DJI has four rotors responsible for vertical takeoff and landing. Digital camera in RGB format with 12.4 megapixels resolution (3000 x 4000), 20 mm focal length and 94 ° viewing angle. It already has a gimbal accessory, which compensates for unwanted movements in the z, x, y (yaw, roll, pitch) axes and adjustable range from 0 to 90 ° in the latter. Payload of 1380 grams, including the battery with real duration of approximately 20 minutes. The flight paths were carried out autonomously, doubly repeated and preprogrammed in the software Pixel4DCapture. Ideally each flight path occurred at 20 meters high, with 96 images collected in the time of 11 minutes, frontal and lateral overlaps of 75 and 76%, pixel of size 0.88 centimeters, camera positioned at 90º in relation to the direction of displacement, balance of black and white automatic and with the option of acquiring images when stopping the aircraft on the waypoints. The discordant values of flight height and spatial resolution along the way are caused by the aircraft float in the airspace (table 1). The differences in the number of images and area covered are consequences of the previous unavailability of saving the flight project, which when reprogrammed by the operator has undergone slight modification, and also because there were differences in the quality of the images, those that presented visibly similar luminosity were selected for further processing. The scheduled time to perform the air operations was the noonday sun.

Table 1. Aspects of project during the autonomous flight.

Aerial Avaliations	Dates (day/month/year)	Number of images	Coverage Area (m^2)	Spatial Resolution (cm/pixel)	Fly height (m)	Time (hours:min) (start - end)
Time 1	23/05/2017	149	8180	0.80	21.3	12:10 – 12:42
Time 2	02/08/2017	134	8500	0.89	23.6	16:14 – 16:26
Time 3	02/09/2017	98	6550	0.80	21.7	12:57 – 13:10
Time 4	21/09/2017	96	7310	0.84	22.5	12:19 – 12:27
Time 5	23/10/2017	73	7430	0.92	24.8	12:15 – 12:18
Time 6	21/11/2017	89	7550	0.84	22.1	13:49 – 14:07
Time 7	29/12/2017	118	8010	0.91	24.2	12:12 – 12:37
Time 8	02/02/2018	156	8100	0.92	24.6	11:47 – 12:17
Time 9	02/03/2018	176	9300	0.94	25.2	14:15 – 14:38
Time 10	31/03/2018	101	7820	0.85	22.8	12:52 – 13:11
Time 11	12/05/2018	140	9420	0.94	25.2	15:11 – 15:40

Source: Own author.

3.4. Georreferencing of Precision

The positioning information obtained by Topcom's GR-3 equipment were in UTM (Universal Transversa Mercator) very useful because the unit of measure of this coordinate system is meters and thus able to make geometric, mathematics and statistics operations in a region. The

Datum SIRGAS is known to establish the geocentric reference system for the americas and the SIRGAS 2000 to establish the geocentric reference system for the Brazilian geodesic system. In table 2, the nine ground control points collected along the field are listed. In order to prepare this data to be read by the Agisoft PhotoScan Professional, we transformed the Datum from SIRGAS 2000 to WGS 84 zone 23 south, because this latter address the region south-east of Brazil, therefore the state of São Paulo and the city of Pirassununga, where the scientific experiment took place.

Table 2. Nine ground control points collected with diferential GPS and exhibited in two different datum.

	Datum SIRGAS 2000 Coordinate Sytem UTM (meters)			Datum WGS 84 and zone 23 south Coordinate System UTM (meters)		
GCPs	Longitude	Latitude	Height	Longitude	Latitude	Height
Base1	246841,584	7570630,325	589,569	-47,45119697	-21,95046893	589,569
GCP1	246825,265	7570652,267	589,538	-47,45135147	-21,95026852	589,538
GCP2	246852,849	7570669,494	587,817	-47,45108191	-21,95011701	587,817
GCP3	246884,009	7570627,453	587,739	-47,45078692	-21,95050098	587,739
GCP4	246856,476	7570609,611	589,413	-47,45105609	-21,95065805	589,413
GCP5	246852,445	7570637,060	588,739	-47,45109084	-21,95040971	588,739
GCP6	246868,043	7570648,852	587,811	-47,45093809	-21,95030552	587,811
GCP7	246871,040	7570666,013	587,201	-47,45090644	-21,95015105	587,201
GCP8	246887,093	7570645,737	587,259	-47,45075425	-21,95033639	587,259

Source: Own author.

The Agisoft PhotoScan Professional also reported the evaluation over accuracy in the positioning system using the root mean squared error (RMSE) over the axis x, y and z (table 3). By the following equations:

$$RMSE_{XY} = \sqrt{\frac{\sum_{i=1}^{n}[(X_{oi} - X_{DGPSi})^2 + (Y_{oi} - Y_{DGPSi})^2]}{n}} \quad (1\text{-a})$$

$$RMSE_{Z} = \sqrt{\frac{\sum_{i=1}^{n}[(Z_{oi} - Z_{DGPSi})^2]}{n}} \quad (1\text{-b})$$

$$RMSE_{TOTAL} = \sqrt{\frac{\sum_{i=1}^{n}[(X_{oi} - X_{DGPSi})^2 + (Y_{oi} - Y_{DGPSi})^2 + (Z_{oi} - Z_{DGPSi})^2]}{n}} \quad (1\text{-c})$$

n : number of control points tested for this project.

X_{Oi},Y_{Oi} : X and Y coordinates measured in the orthophoto for the ith control point.

X_{DGPSi},Y_{DGPSi} : X and Y coordinates measured with diferential GPS for the ith control point.

Z_{Oi} is the height in the ith control point, derived from digital soil model

Z_{DGPSi} : Z coordinate of the ith control point measured with diferential GPS

Similar assessment of photogrammetric mapping accuracy was obtained by Aguera-Vega in 2017 (Aguera-Vega, 2017), he flyed at 120 meters of altitude over 17.64 hectares and captured 160 images, corrected with fifteen ground control points.

Table 3. Accuracy on geographical positions evaluated by root mean squared error (RMSE), on the axis xy, z, total and pixel.

Aerial Avaliations	RMSExy (cm)	RMSEz (cm)	RMSEtotal (cm)	RMSEpixel
Tempo 1	1.46	11.55	11.64	0.665
Tempo 2	6.77	17.07	18.37	0.890
Tempo 3	2.44	4.15	4.71	0.459
Tempo 4	3.12	3.21	4.47	0.447
Tempo 5	2.02	4.38	4.83	0.359
Tempo 6	1.63	0.86	1.84	0.321
Tempo 7	1.36	3.45	3.70	0.332
Tempo 8	9.26	15.19	17.79	3.036
Tempo 9	3.25	5.88	6.72	0.853
Tempo 10	1.88	4.37	4.75	0.284
Tempo 11	4.85	6.42	8.05	1.031

Source: Own author.

3.5. Orthomosaic Contruction

The Universal Transverse Mercator (UTM) coordinate system (Zone 23S, WGS84, EPSG:32723) West-East and South-North of the analyzed area were (246800, 246916) and (7570585, 7570700), respectively. The orthomosaic of dimensions 116 x 115 m (13340 m²) and spatial resolution set to 1 cm per pixel was produced by overlap of RGB images, therefore the orthomosaic contained 116000 x 115000 pixels, and the mosaicing was executed in the comercial low-cost software Agisoft PhotoScan Professional photogrammetric mapping, for this procedure a high performance machine was necessary, we used an Intel Core i7-6700HQ CPU, with a 2.60 GHz processor, 32GB of RAM memory and video card NVIDIA GeForce GTX 1070.

The software Agisoft PhotoScan Professional is capable of creating from a series of overlapping images, the sparse cloud, dense point cloud, three-dimensional texture meshes, three-dimensional (3D) contents, digital soil model, and orthomosaics, becoming a powerful tool nowadays for cultural heritage surveys and documentations (Chiabrando *et al.*, 2015). There are two main algorithms used in this process, the first is the Structure from Motion (SfM), responsible for the great innovation in the image matching process related to photogrammetry, which allows the collection of information at different heights and directions, enables alignment and calibration of the images, through automatic identification of matching features (Aguera-Vega et al., 2017). The second is similar to the Scale Invariant Feature Transform (SIFT) that was developed by Lowe in

2004 (since this is protected by the copyright), and is responsible for the extraction of feature points and fit the overlapping images, forming the cloud of points (Chiabrando *et al.*, 2015, Weiss e Baret, 2017) .

The first phase of the orthomosaic construction is the alignment of the images, this was set to high accuracy and pair pre-selection using the ground control points. The dense cloud points with high quality and depth filtering agressive were built next. Then the mesh with arbitrary surface type was done, high face count and dense cloud point as source data. Afterwards the texture with generic mapping mode, mosaic blending mode and texture size/count to 4096. Finally the orthomosaic with datum type set to WGS 84/UTM zone 23S (EPSG::32723) was created, pixel size of 1 cm, and was exported with setup boundaries from 246800 to 246916 in the x-axis and from 7570585 to 7570700 in the y-axis. It's worthy to point out that this last stage is the most sensitive (table 4).

Table 4. Time consumed to construct the steps that lead to orthomosaic.

Aerial Avaliations	Number of images	Alignment (min)	Dense Cloud Points (h)	Mesh (min)	Texture (min)	Orthomosaic (min)	Total time (h)
Time 1	149	21.05	4.75	27.55	10.51	2.75	5.78
Time 2	134	17.45	4.95	21.38	4.98	2.25	5.72
Time 3	98	9.15	1.23	24.00	9.53	2.08	1.98
Time 4	96	13.50	1.29	20.37	8.42	1.82	2.02
Time 5	73	7.03	1.25	18.15	12.11	1.53	1.90
Time 6	89	7.61	0.77	27.00	19.53	2.07	1.71
Time 7	118	21.43	4.21	21.75	18.80	2.30	5.28
Time 8	156	25.68	4.50	22.88	16.27	3.03	5.64
Time 9	176	30.71	8.35	22.25	10.22	3.45	9.46
Time 10	101	9.77	1.86	25.83	15.32	2.42	2.75
Time 11	140	14	3.84	25.33	13.45	2.7	4.76

Source: Own author.

3.6. Set Theory and Algebraic Maps

Sets are fundamental concepts of mathematics and science. Referring to the classic notes, according to Cantor (1883), set is discribed as "any multiplicity, which can be thought of as one...any totality of definite elements, which can be bound up into a whole by means of a law" (apud Pedrycz and Gomide, 2007).

Fuzzy sets offer an important and unique feature of describing information granules whose contributing elements may belong to varying degrees of membership. This helps us describe the concepts that are commonly encountered in the real world (Pedrycz and Gomide, 2007).

In the 1930s, the Comission Internationale d'Eclairage (CIE) standardized the RGB representation by peforming such color matching experiments using primary colors of red (700.0nm wavelength), green (546.1nm), and blue (435.8nm).

(a) (b)

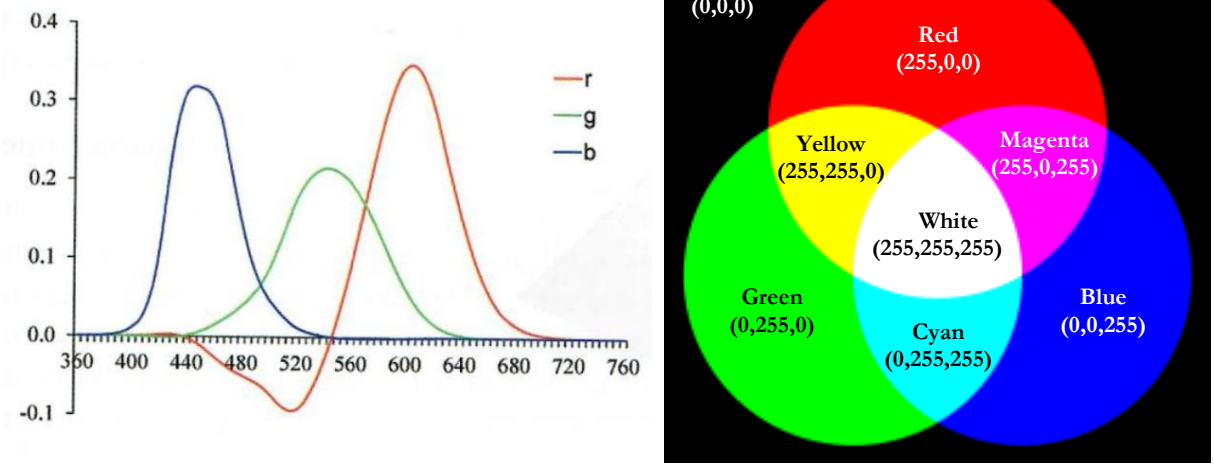

Figure 3. a) Standard CIE color spectra obtained from pure colors to the R=700.0 nm, G=546.1nm and B=435.8nm (Source: Szeliski, 2011). b) additive color model RGB (red, green and blue) can be mixed to produce cyan, magenta, yellow and white (Adapted from Szeliski, 2011).

Universe of discourse:

$$Red = \{ x \epsilon \mathbb{N} \mid 0 \leq x \leq 255 \}$$

$$Green = \{ x \epsilon \mathbb{N} \mid 0 \leq x \leq 255 \}$$

$$Blue = \{ x \epsilon \mathbb{N} \mid 0 \leq x \leq 255 \}$$

$$RGB = Red \cup (Green \cup Blue)$$

Subset (Halmos, 1960):

$$Red \subset RGB \ because \ Red \cup RGB = RGB$$

$$Green \subset RGB \ because \ Green \cup RGB = RGB$$

$$Blue \subset RGB \ because \ Blue \cup RGB = RGB$$

$$Red \subset RGB \ because \ Red \cap RGB = Red$$

$$Green \subset RGB \ because \ Green \cap RGB = Green$$

$$Blue \subset RGB \ because \ Blue \cap RGB = Blue$$

Classical theory (Halmos, 1960):

$$A \cap B = \{ x \mid x \in A \; e \; x \in B \}$$

Fuzzy theory :

$$\mu_A(x) \cap \mu_B(x) = \min\{ \mu_A(x), \mu_B(x) \}$$

In this passage we used the fuzzy technique of sets intersection. We entered with a RGB image and strategically placed a white (255,255,255) and a black (0,0,0) image as a filter, in this way the values in contact with the white part of the image are maintained, while the black values are prevailed in the resulting image (figure 4). This is a very efficient technique for information display and may be applied in several purposes with the spatialized information that have minimal error within geographic positioning.

(a)

(20, 33, 175)	(25, 31, 13)	(85, 219, 77)	(18, 169, 250)
(80, 175, 230)	(10, 110, 220)	(33, 144, 230)	(13, 15, 13)
(15, 38, 23)	(56, 88, 155)	(99, 87, 150)	(79, 68, 197)
(149, 67, 165)	(14, 69, 82)	(46, 29, 37)	(88, 248, 269)

$\cap$

(b)

(0,0,0)	(0,0,0)	(0,0,0)	(0,0,0)
(0,0,0)	(255, 255, 255)	(255, 255, 255)	(0,0,0)
(0,0,0)	(255, 255, 255)	(255, 255, 255)	(0,0,0)
(0,0,0)	(0,0,0)	(0,0,0)	(0,0,0)

$=$

(c)

(0,0,0)	(0,0,0)	(0,0,0)	(0,0,0)
(0,0,0)	(10, 110, 220)	(33, 144, 230)	(0,0,0)
(0,0,0)	(56, 88, 155)	(99, 87, 150)	(0,0,0)
(0,0,0)	(0,0,0)	(0,0,0)	(0,0,0)

Figure 4. Simulation in numeric values of an interseccion between a (a) RGB image and a (b) black and white image. Source: Own author.

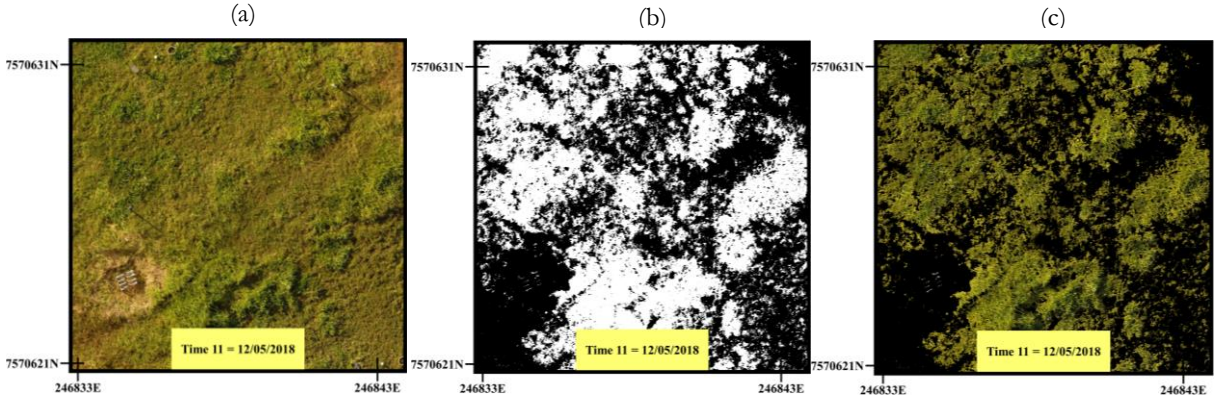

Figure 5. The intersection among a (a) RGB image and a (b) black and white image, this procedure highlight only the (c) image with desired values. Source: Own author.

Set theory and algebraic maps form a tool that has huge advantage for spatial analysis of attributes. For example, at the beginning of a crop cycle, after an aerial avaliation the first digital elevation model (figure 7a) was formed. After 66 days a new aerial avaliation occurred and therefore a creation of a new planialtimetric model (figure7b). To infer the growth of this crop, the use of mathematical operation of subtraction between the first and second aerial avaliaton (figure 7c) was necessary. It is important to emphasize that to know the height of a culture along the time is necessary to make an aerial evaluation before the vegetation begins to grow, so it is possible to subtract the height of the crop from the terrain within the geographic positioning.

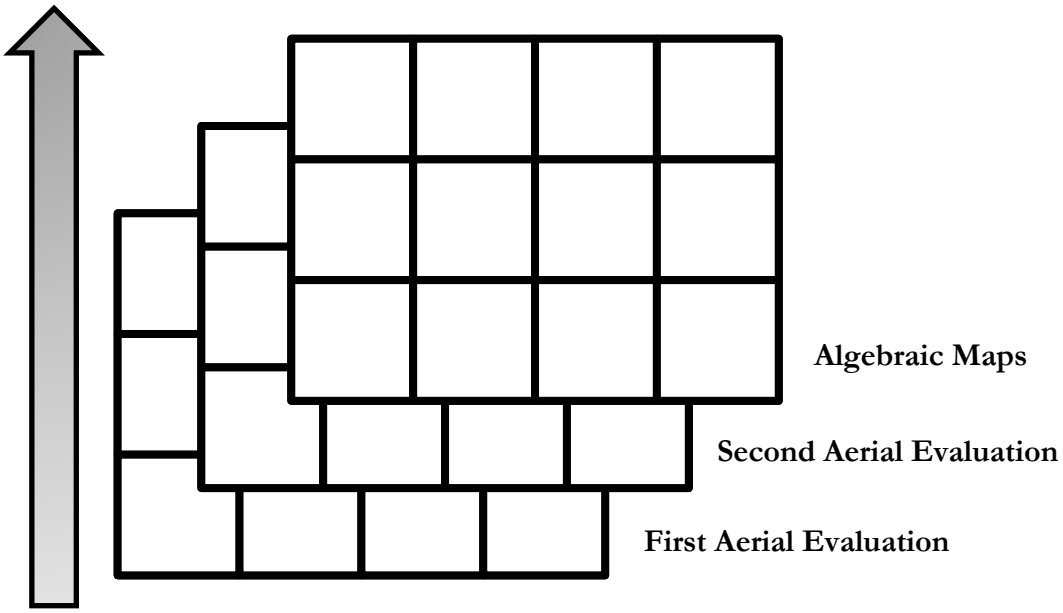

Figure 6. Computacional algorithm advancing through the time. Source: Own author.

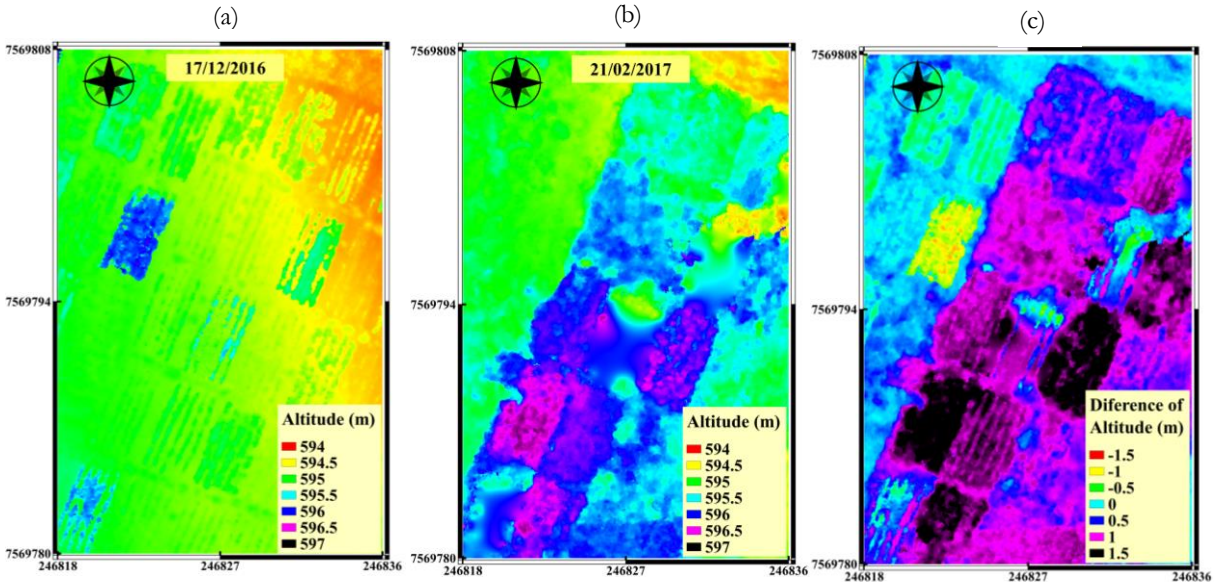

Figure 7. (a) First aerial evaluation, (b) Second aerial evaluation (c) The subtraction between the second and the fisrt digital elevation models, and therefore the vertical growth of the crop. Source: Own author.

3.7. Area Rotulation and Delimitation

The creation of square polygons with 100 m² (10 m x 10 m) that delimited the plots of the field treatments were fistly made in the QGIS georeferencing software (Figure 8a), since the operations are projected in toolbox forms and, therefore, easier to implement. Next there was the clipping of raster map RGB with 20 identical sizes polygons, highlighting the areas related to each plot, this image was exported in TIF file (Figure 8b), the pixel size remained 0.1 centimeters, the geographical coordinates system was UTM WGS-84 Zone 23 and ranged between (246800, 246916) for longitude and (7570585, 7570700) for latitude, resulting in an image size of 11600 x 11500 pixels.

The creation of the square polygons occurred again, this time in Python software 2.7.13, with reference of the image produced by the QGIS software. In this way there was the spatial guarantee between the processes executed in the different softwares (figure 9a and 9b). The reverse path (Python → QGIS) is also possible by the use of the georeferencing tool (QGIS), and for the reliable adoption of this practice it is necessary to have minimal errors within the geographic positioning, which were achieved in this work (table 3).

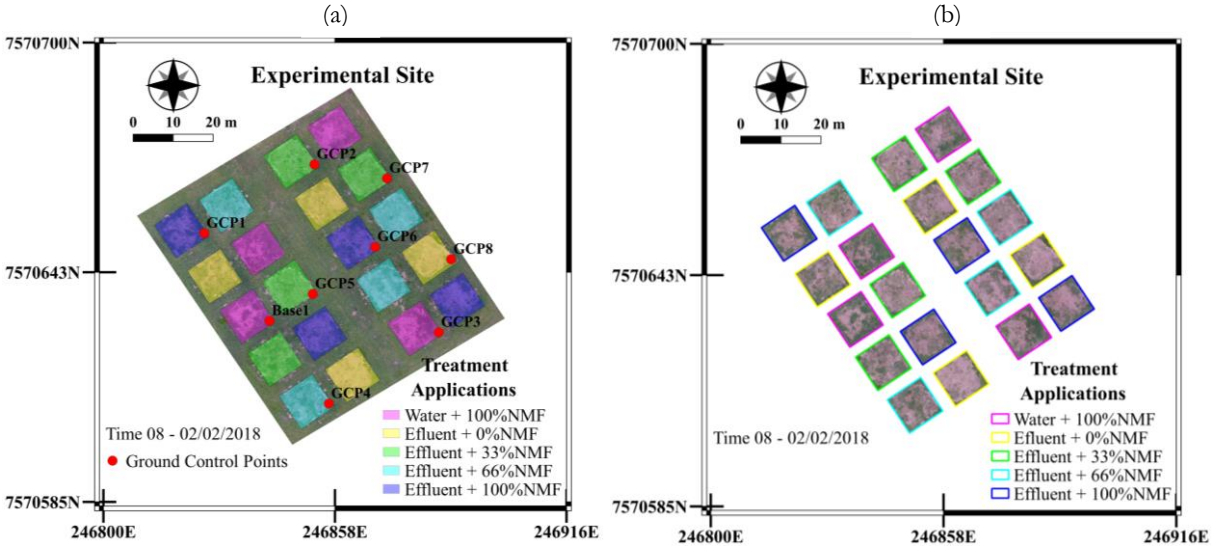

Figure 8. a) Image displayed at the software QGIS b) The same image after be clipped by a mask layer of all parcels. Source: Own author.

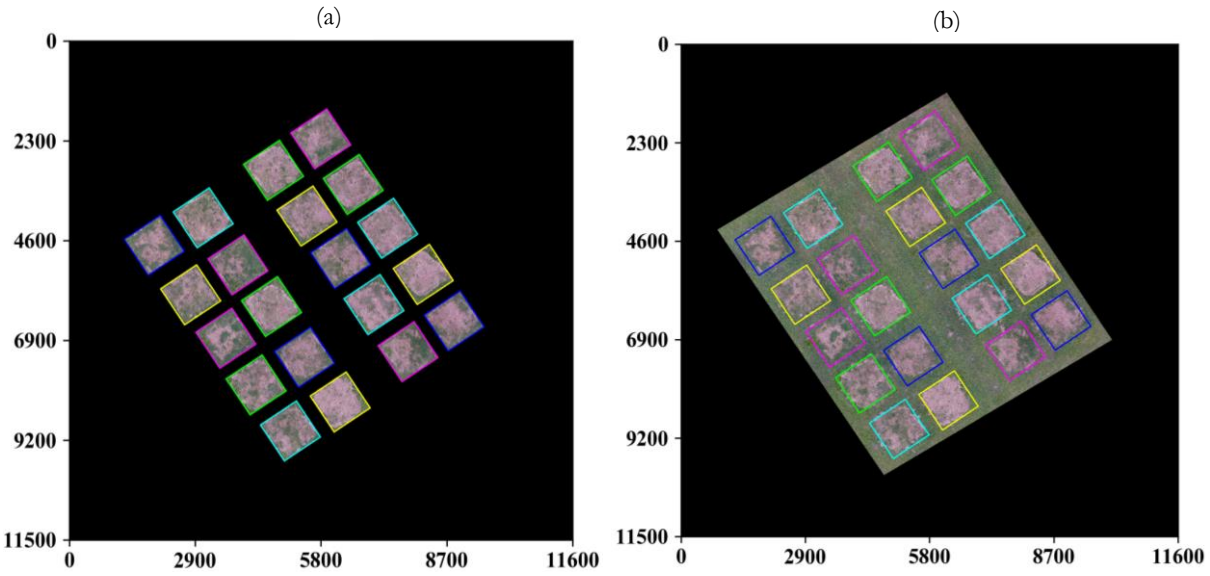

Figure 9. a) The image previously clipped by a mask here is used to adjust the polygon arrays in the software Python 2.7.13. b) The image become compatible spatially, integration between QGIS and Python is reached. Source: Own author.

3.8. Transformation from RGB to HSV

The color space RGB (Red, Green, Blue) is widely used in vision systems in machines, although their components are strongly correlated and vary with lighting conditions and therefore not recommended to work in outdoor fields (Meng et al., 2015). The HSV color space (Hue, Saturation, Value) is developed to approximate the human way of perceiving colors. The component V (value) indicates the level of illumination or brightness of the color, H (hue) defines the color itself or the spectral range (e.g. pure red, yellow or cyan), and S (saturation) indicates the purity of the color or how much it is diluted in white light (Yang et al., 2015, Hamuda et al., 2017).Within a primary color cube with edge length 255, the major diagonal line connecting the origin to the farthest vertex is called the gray line because the pixels in this line have the same value in red, green and blue. After using the equations 2-a, 2-b, 3 and 4, a nonlinear transformation of color spaces occurs, changing from RGB color cube to HSV color cone (Forsyth and Ponce, 2003). In this new arrangement the hue provides the spectral description in the form of an angle ranging from 0 to 360 ° and should be re-scaled in 8 bits [0, 255] natural values for color arrangement.

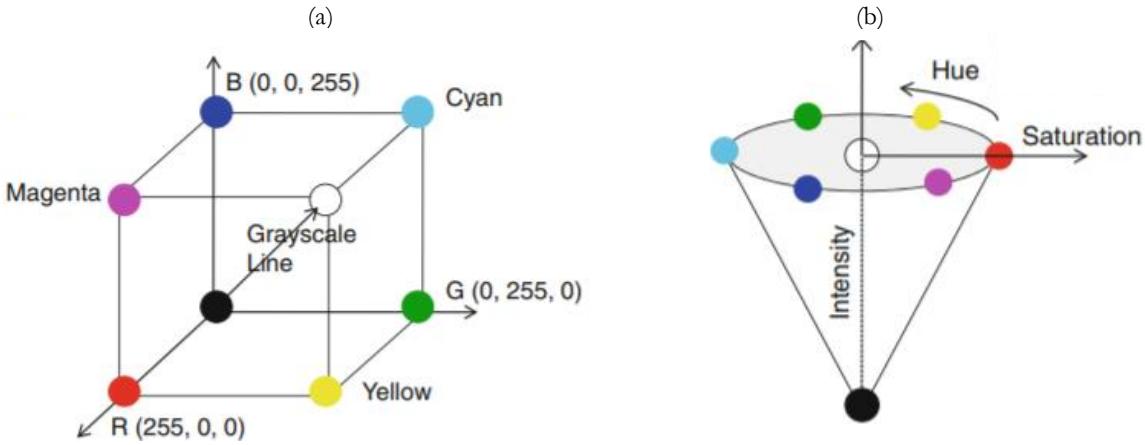

Figure 10. Nonlinear transformation from (a) RGB color cube to (b) HSV color cone (Source: Mendoza and Lu, 2015)

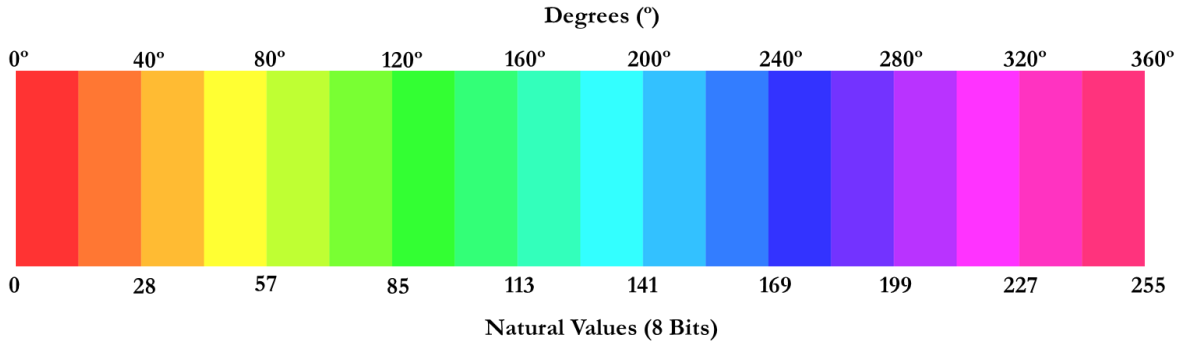

Figure 11. Hue color arrangement. For this representation the saturation and value are fixed on the unit value. Source: Own author.

$$H = \begin{cases} \theta & ,if\ B \leq G \\ 360 - \theta & ,if\ B > G \end{cases} \quad (2\text{-a})$$

$$\theta = \arccos\left\{\frac{[(R-G)+(R-B)]/2}{[(R-G)^2+(R-G)(G-B)]^{1/2}}\right\} \quad (2\text{-b})$$

$$S = 1 - \frac{3}{(R+G+B)}[\min(R,G,B)] \quad (3)$$

$$V = \frac{1}{3}(R+G+B) \quad (4)$$

3.9. Graphical Models, Decision Trees and Rules

Graphical models represent the interaction between variables visually and have the advantage that inference over a large number of variables can be decomposed into a set of local calculations involving a small number of variables making use of conditional independencies. The analysis using diagrammatic representations of probability distributions, called probabilistic graphical models, play a central role in modern pattern recognition and offer several useful properties (Bishop, 2006; Alpaydin, 2010):

1- They provide a simple way to visualize the structure of a probabilistic model and can be used to design and motivate new models.
2- Insights into the properties of the model, including conditional independence properties, can be obtained by inspetion of the graph.
3- Complex computations, required to perform inference and learning in sophisticated models, can be expressed in terms of graphical manipulations in which underlying mathematical expressions are carried along implicity.

A decision tree is a hierarchical model for supervised learning, the network is a direct acyclic graph whose nodes are marked by a random attribute X (input variable) and links are associated with conditional probability P(X|Y) from node X to node Y. The conditional probabilities are the parameters given the structure and indicates that X has a direct influence on Y. The termial nodes concern the values of the output variable (Bishop, 2006).

A decision tree is also a nonparametric model in the sense that we do not assume any parametric form for the class densities and the tree structure is not fixed previously but the tree grows, branches and leaves are added during learning depending on the complexity of the problem inherent in the data. Another advantage of the decision trees is interpretability, the tree can be converted to a set of IF-THEN rules that are easily understandable (Alpaydin, 2010).

Each rule can be interpreted as an individual local descriptor of the data (problem), and the quality may be evaluated under granularity of condition and granularity of conclusion. The high granularity condition (very specific), comes up with the rule that is very limited and confined to some small region in the input space. When the granularity of condition decreases, the generality of the rule increases, and this rule could be applied to more situations (Pedrycz and Gomide, 2007)

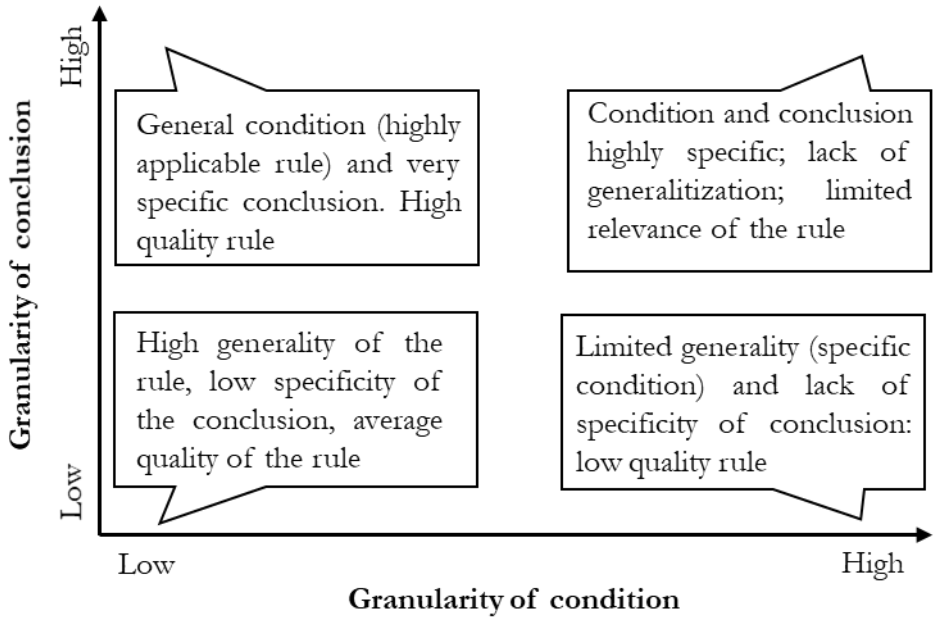

Figure 12. Rules interpretability (Source: Pedrycz and Gomide, 2007)

3.10. K-means algortihm

The K-means algorithm is a nonprobabilistic technique to find clusters in a set of data points (Lloyde, 1982). A general technique for finding maximum likelihood estimators in latent variables models is the expectation-maximization (EM) algorithm. The K-means algorithm corresponds to a particular nonprobabilistic limit of EM applied to mixture of Gaussians (Bishop, 2006).

4. RESULTS AND DISCUSSION

4.1. Eighth Aerial Evaluation

The following discussion shows the eighth aerial evaluation analyzed through the methodology explained in figure 1. First the georeferenced thematic map displaying the RGB channels was automated, thus all the orthomosaic constructed within this area were predefined with the same frame of the geographical information system (figures 13-a and 17-a). Then in the software Python occurred the transformation from RGB to HSV color space and the hue channel was selected, and on it was applied the k-means algorithm with 6 clusters (figure 13-b and 17-b).

The orthomosaic with hue channel grouped with 6 clusters of k-means was lead to software QGIS through the "georeferencer" tool, and in this platform received the coloration of the hue space (figure 11) according to the values received by the centers of the k-means clusters (figure 14-a and 18-a). The histogram that contains the density probability function of hue color space along the field is showed in the figure 14-b and 18-b.

By human visual comparison we joined the clusters 1, 2 and 6 to form the soil and the clusters 3, 4 and 5 to form the vegetation. By previous demonstrations (Chapter 3.6) we deduced that Cluster 1 $\subset$ Soil, Cluster 2 $\subset$ Soil, Cluster 6 $\subset$ Soil, Cluster 3 $\subset$ Vegetation, Cluster 4 $\subset$ Vegetation, Cluster 5 $\subset$ Vegetation (figure 15a and 15b). In this representation related above, the description of the vegetation group was represented by three different subgroups, that represented coloration differences between them. And the same happened to the soil group, that was represented by three diferente subgroups, with differences in colorations between each other. Cluster 1 corresponded to red color, cluster 2 to orange red color, cluster 3 to orange color, cluster 4 to spring bud color, cluster 5 to lawn green color and cluster 6 to navy blue color (figure 14a and 14b).

Previously (Chapter 3.7) the area of 100 m^2 for each portion was delimited, and the probability density function had to sum a total of 100%, so we had the direct relation of 1m^2 to 1% in each portion. We worked with a supervised method of learning where the inputs were the repetition of each treatment multiplied by the number of treatments (four repetitions x five treatments = twenty instances), the attributes were the clusters of the hue colors centered by the k-means algorithm and the five treatments were the outputs of our system (table 5 and 9).

After the hue channel grouped with 6 clusters of the k-means algorithm had been exported in txt format by the Python software, it was arranged in tabular information in Excel and then lead as csv format to the Weka software where the decision tree algorithm (figure 16 and 20)

was applied. Although this algorithm had been evaluated over the training set, it presented accuracy of 85% for a first decision tree and a higher accuracy of 100% for the second although the complexity of the system also increased (table 6 and 8).

In the eighth aerial evaluation the rule that lead to water treatment (W100) was examinated, for this case the cluster5 > 10.05 and cluster2 <=7.61 and cluster4 >12.24 and cluster2 <= 6.29. Previously it was induced that the knowledge that cluster 5 and cluster 4 belonged to vegetation group while cluster 2 was set to soil group. Therefore in this evaluation time there was more vegetation and less soil in W100 than in another treatments.

Accordingly to Yang (2015) many researchers have also used methods based on visible spectral-index (ExG, ExGR, VEG, CIVE, COM) in an attempt to identify the greenness of agricultural crops, but these indices are efficient under the clear contrast assumption of plants with high greenness and exposed soil, whereas the identification of greenness based on HSV provides a more robust method, because in agriculure the background elements may contain crop straw, straw ash besides soil and the color of the plants varies from dark green to bright green.

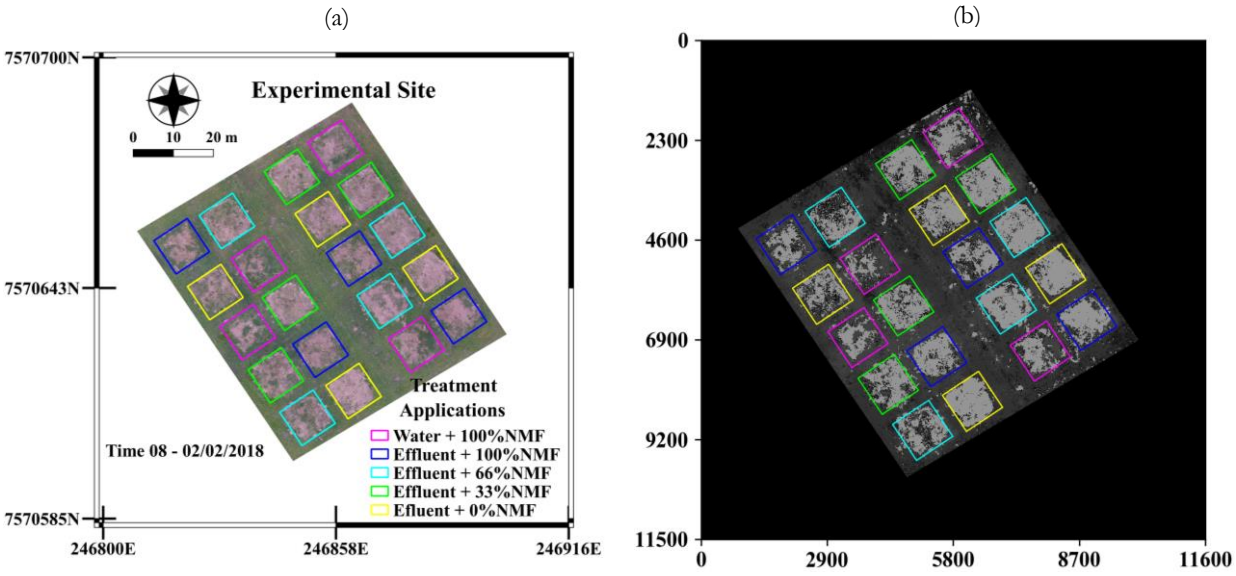

Figure 13. Eighth aerial evaluation. a) Georeferenced thematic map with RGB channels displayed in software QGIS. b) Orthomosaic transformed to hue channel and displayed in the software Python. W100 - water irrigation with 100% of nitrogen mineral fertilization; E0, E33, E66 and E100 - irrigation with treated effluent from slaughterhouse and addition of 0, 33; 66 and 100% nitrogen mineral fertilization, respectively. Source: Own author.

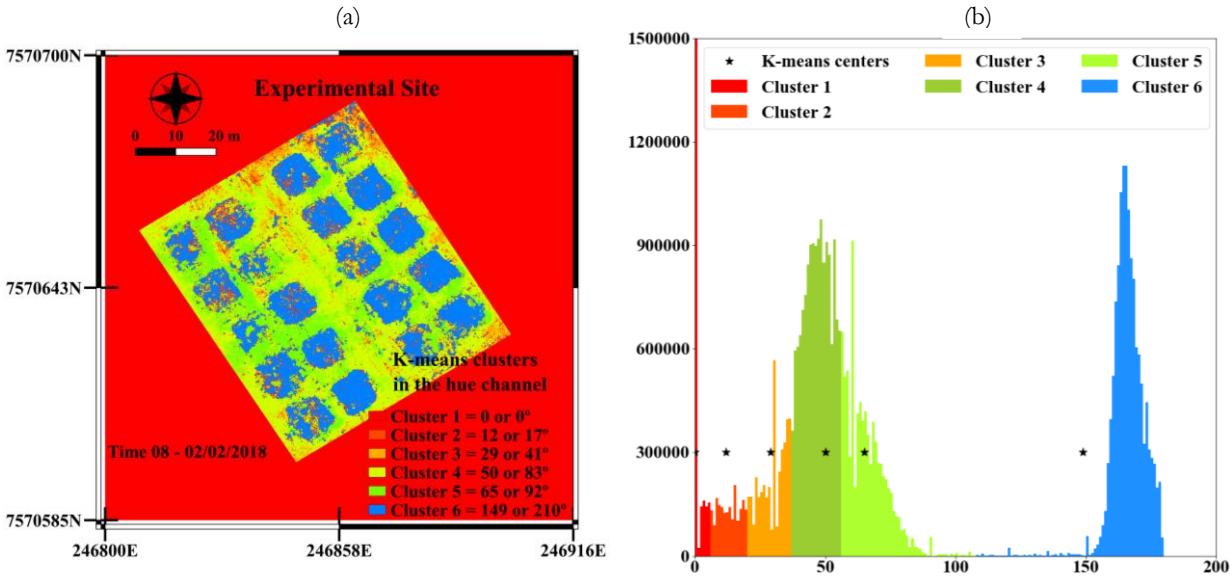

Figure 14. Eighth aerial evaluation. a) Georeferenced thematic map with the hue channel grouped by 6 clusters of k-means algorithm. b) Histogram of the hue channel representing the field of study, grouped and displayed by 6 k-means centers. Source: Own author.

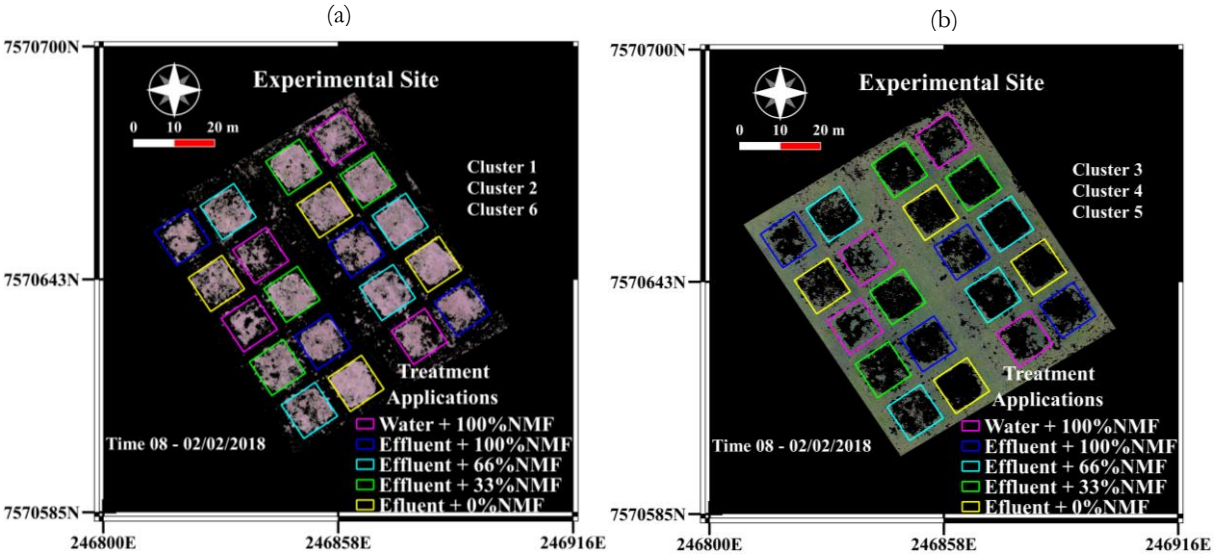

Figure 15. Eighth aerial evaluation. a) Georeferenced thematic map with three clusters that together defined the soil b) Georeferenced thematic map with three cluster that together defined the vegetation. W100 - water irrigation with 100% of nitrogen mineral fertilization; E0, E33, E66 and E100 - irrigation with treated effluent from slaughterhouse and addition of 0, 33; 66 and 100% nitrogen mineral fertilization, respectively. Source: Own author

Table 5. Eighth aerial evaluation. Percentage of found patterns inside each parcel in terms of hue clusters.

Treatment	Probability Density Function (%)					
Applications	Cluster2	Cluster3	Cluster4	Cluster5	Cluster6	Sum
E0	9.11	6.05	12.11	18.18	54.56	100
E0	2.81	2.98	12.24	2.98	79	100
E0	6.66	4.94	13.14	5.82	69.44	100
E0	3.23	3.1	9.67	8.5	75.5	100
E33	7.16	5.32	10.63	9.76	67.13	100
E33	6.18	4.31	9.62	6.81	73.08	100
E33	6.81	5.34	13.12	3.18	71.55	100
E33	3.46	2.7	8.3	5.98	79.55	100
E66	8.06	7.38	14.32	12.36	57.88	100
E66	12.85	9.34	14.79	6.8	56.22	100
E66	2.92	3.12	9.6	10.05	74.31	100
E66	3.13	2.3	7.25	5.61	81.71	100
E100	6.6	5.35	14.44	28.83	44.79	100
E100	4.51	3.42	10.83	17.05	64.19	100
E100	7.36	7.95	17.2	11.26	56.23	100
E100	3.53	4.05	11.14	13.21	68.07	100
W100	2.9	3.48	14.25	42.36	37.01	100
W100	5.47	7.07	26.06	32.4	28.99	100
W100	6.29	7.21	19.55	18.47	48.47	100
W100	7.61	9.19	14.57	10.24	58.38	100

Source: Own author.

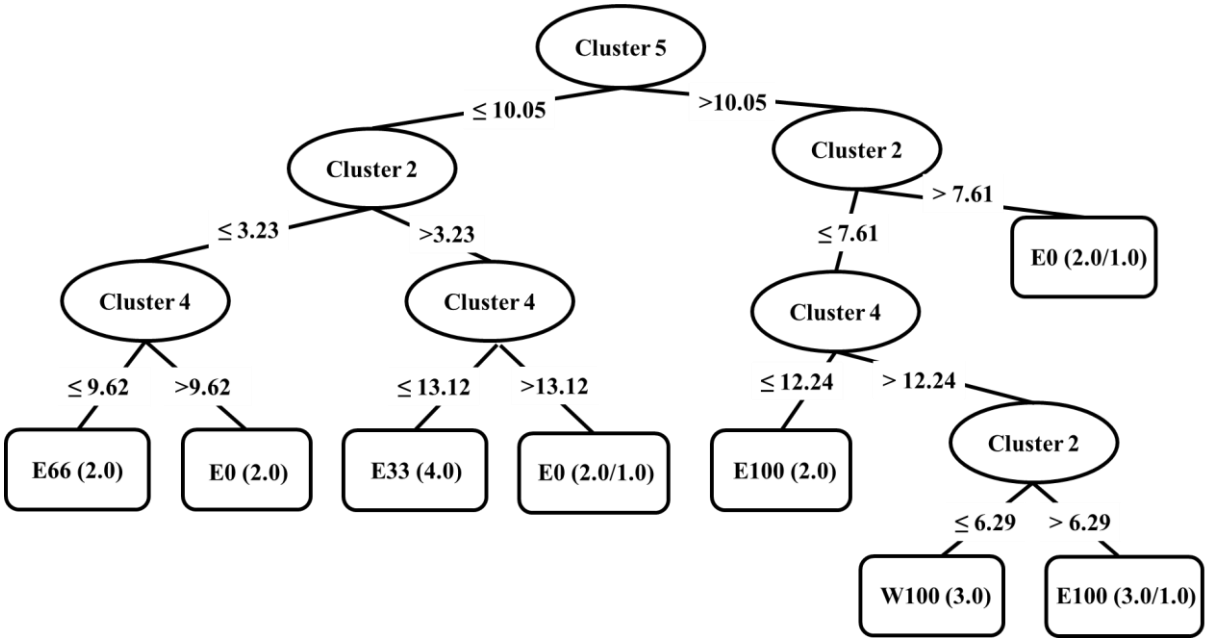

Figure 16. Eighth aerial evaluation. Decision tree that explored the paths that recognized the wastewater treatments. Source: Own author.

Table 6. Eighth aerial evaluation. Confusion matrix evaluating the classifier.

Confusion Matrix		Predicted Class				
		E0	**E33**	**E66**	**E100**	**W100**
Actual Class	**E0**	4	0	0	0	0
	E33	0	4	0	0	0
	E66	2	0	2	0	0
	E100	0	0	0	4	0
	W100	0	0	0	1	3

Source: Own author.

Table 7. Eighth aerial evaluation. Decision tree outputs about the size and complexity of the system.

Aerial Evaluation	Color Space	First Decision Tree			Second Decision Tree		
		Accuracy	**Leaves**	**Nodes**	**Accuracy**	**Leaves**	**Nodes**
Time 08	Hue	85%	8	15	100%	10	19

Source: Own author.

Table 8. Eighth aerial evaluation. Paths that led to leaves of decision tree transformed into a set of rules.

If Cluster5 > 10.05 and Cluster2 > 7.61 E0
If Cluster5 > 10.05 and Cluster2 <= 7.61 and Cluster4 <= 12.24 then E100
If Cluster5 > 10.05 and Cluster2 <= 7.61 and Cluster4 >12.24 and Cluster2 <= 6.29 then W100
If Cluster5 > 10.05 and Cluster2 <= 7.61 and Cluster4 >12.24 and Cluster2 > 6.29 then E100
If Cluster5 <= 10.05 and Cluster2 <= 3.23 and Cluster4 <= 9.62 then E66
If Cluster5 <= 10.05 and Cluster2 <= 3.23 and Cluster4 > 9.62 then E0
If Cluster5 <= 10.05 and Cluster2 > 3.23 and Cluster4 <= 13.12 then E33
If Cluster5 <= 10.05 and Cluster2 > 3.23 and Cluster4 > 13.12 then E0

Source: Own author

4.2. Ninth Aerial Evaluation

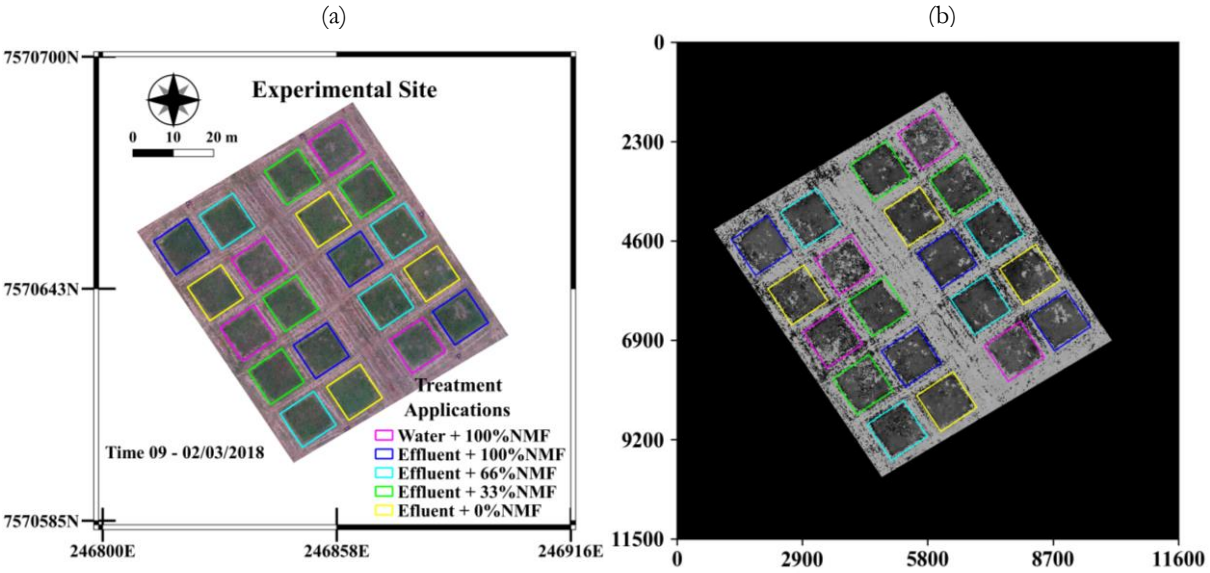

Figure 17. Ninth aerial evaluation. a) Georeferenced thematic map with channels RGB displayed in software QGIS. b) Orthomosaic transformed to hue channel and displayed in the software Python. W100 - water irrigation with 100% of nitrogen mineral fertilization; E0, E33, E66 and E100 - irrigation with treated effluent from slaughterhouse and addition of 0, 33; 66 and 100% nitrogen mineral fertilization, respectively. Source: Own author.

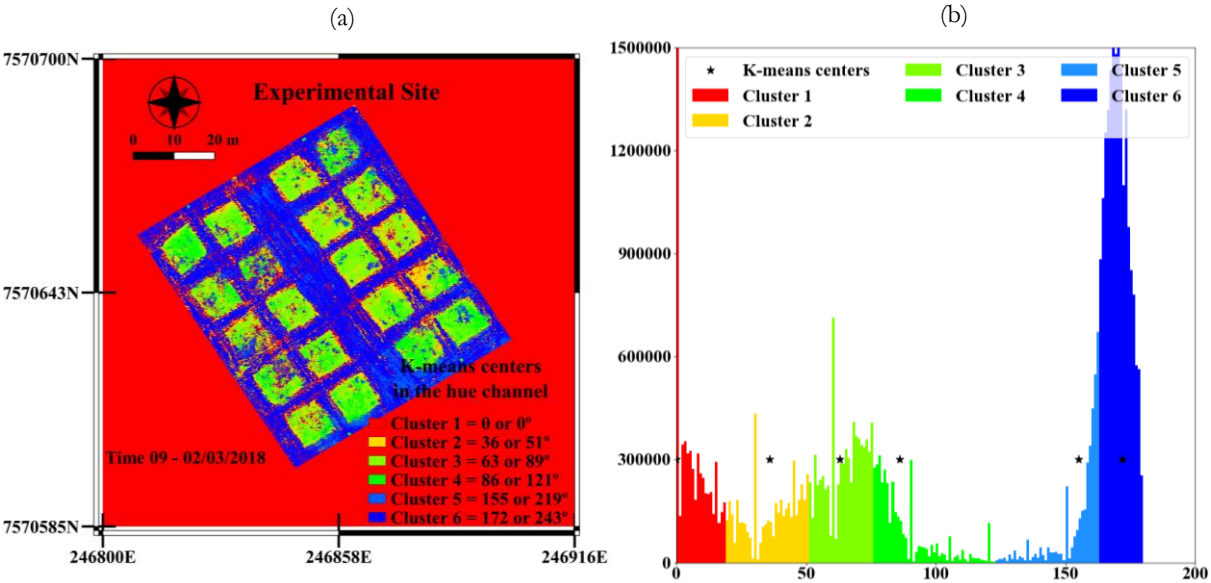

Figure 18. Ninth aerial evaluation. a) Georeferenced thematic map with the hue channel grouped by 6 clusters of k-means algorithm. b) Histogram of the hue channel representing the field of study, grouped by 6 k-means clusters centers. Source: Own author.

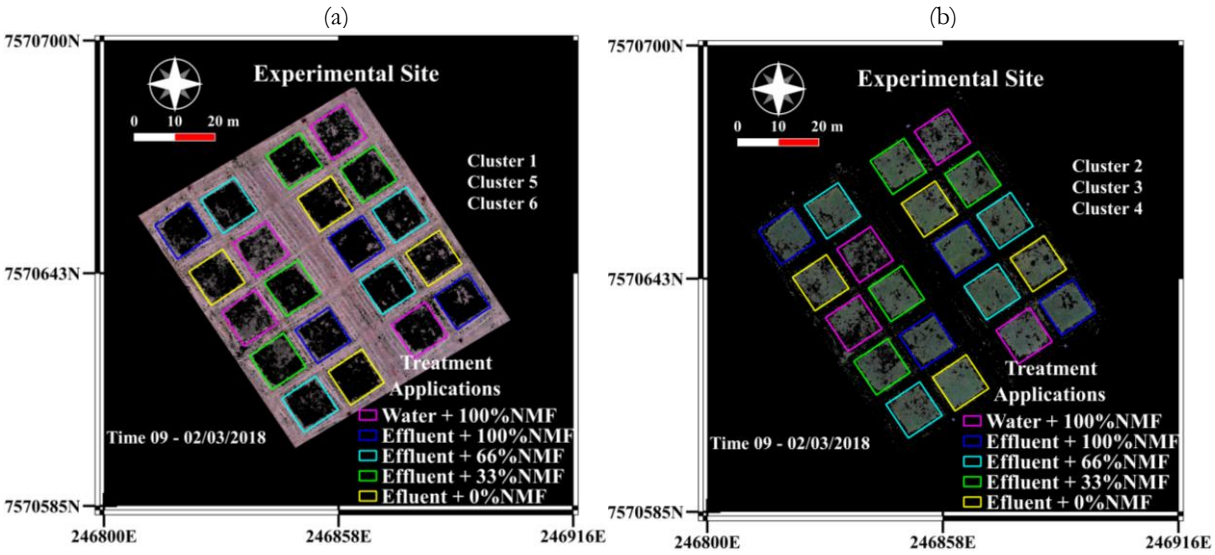

Figure 19. Ninth aerial evaluation. a) Georeferenced thematic map with three clusters that together defined the soil. b) Georeferenced thematic map with three cluster that together defined the vegetation. W100 - water irrigation with 100% of nitrogen mineral fertilization; E0, E33, E66 and E100 - irrigation with treated effluent from slaughterhouse and addition of 0, 33; 66 and 100% nitrogen mineral fertilization, respectively. Source: Own author.

By human visual comparison we joined the clusters 1, 5 and 6 to form the soil and the clusters 2, 3 and 4 to form the vegetation. By previous demonstrations (Chapter 3.6) we deduced that Cluster 1 ⊂ Soil, Cluster 5 ⊂ Soil, Cluster 6 ⊂ Soil, Cluster 2 ⊂ Vegetation, Cluster 3 ⊂ Vegetation, Cluster 4 ⊂ Vegetation (figure 19a and 19b). In this representation related above, the description of the vegetation group was represented by three different subgroups, that represented coloration differences between them. And the same happened to the soil group, that was represented by three diferente subgroups, with differences in colorations between each other. Cluster 1 corresponded to red color, cluster 2 to golden yellow color, cluster 3 to chartreuse color, cluster 4 to lime color, cluster 5 to navy blue color and cluster 6 to blue color (figure 18a and 18b).

The decision tree algorithm (figure 20) was applied. Although this algorithm had been evaluated over the training set, it presented accuracy of 85% for a first decision tree and a higher accuracy of 100% for the second although the complexity of the system also increased (table 8).

In the nineth aerial evaluation the rule that lead to water treatment (W100) was of general condition (highly applicable rule), for this case the cluster3 ≤ 26.65. Previously it was induced that the knowledge that cluster 3 belonged to vegetation group. Therefore in this evaluation time there was less vegetation with this spectral range in W100 than in another treatments.

Table 9. Ninth aerial evaluation. Percentage of found patterns inside each parcel in terms of hue clusters.

Treatment Applications	Probability Density Function (%)					
	Cluster 2	Cluster 3	Cluster 4	Cluster 5	Cluster 6	Sum
E0	20,91	37,4	19,73	7,33	14,63	100
E0	9,65	47,05	31,1	5,82	6,38	100
E0	28,02	51,68	5,63	5,66	9,01	100
E0	33,17	29,17	15,56	7,21	14,9	100
E33	16,91	33,23	23,69	7,63	18,55	100
E33	18,28	49,89	12,64	5,01	14,17	100
E33	24,88	48,66	9,6	3,6	13,26	100
E33	21,83	46,99	13,54	6,81	10,83	100
E66	23,12	38,28	18,4	6,65	13,55	100
E66	18,82	44,91	18,37	4,31	13,59	100
E66	24,24	49,29	17,31	2,7	6,46	100
E66	34,79	46,7	3,66	1,72	13,13	100
E100	10,78	28,35	41,53	5,61	13,73	100
E100	18,42	41,96	21,2	3,19	15,23	100
E100	18,5	60,56	8,98	3,41	8,55	100
E100	7,12	39,78	35,16	10,63	7,31	100
W100	28,74	24,7	9,53	11,18	25,85	100
W100	19,06	12,31	15,08	16,86	36,68	100
W100	10,8	26,65	40,69	14,6	7,27	100
W100	13,7	19,04	28,92	21,15	17,19	100

Source: Own author.

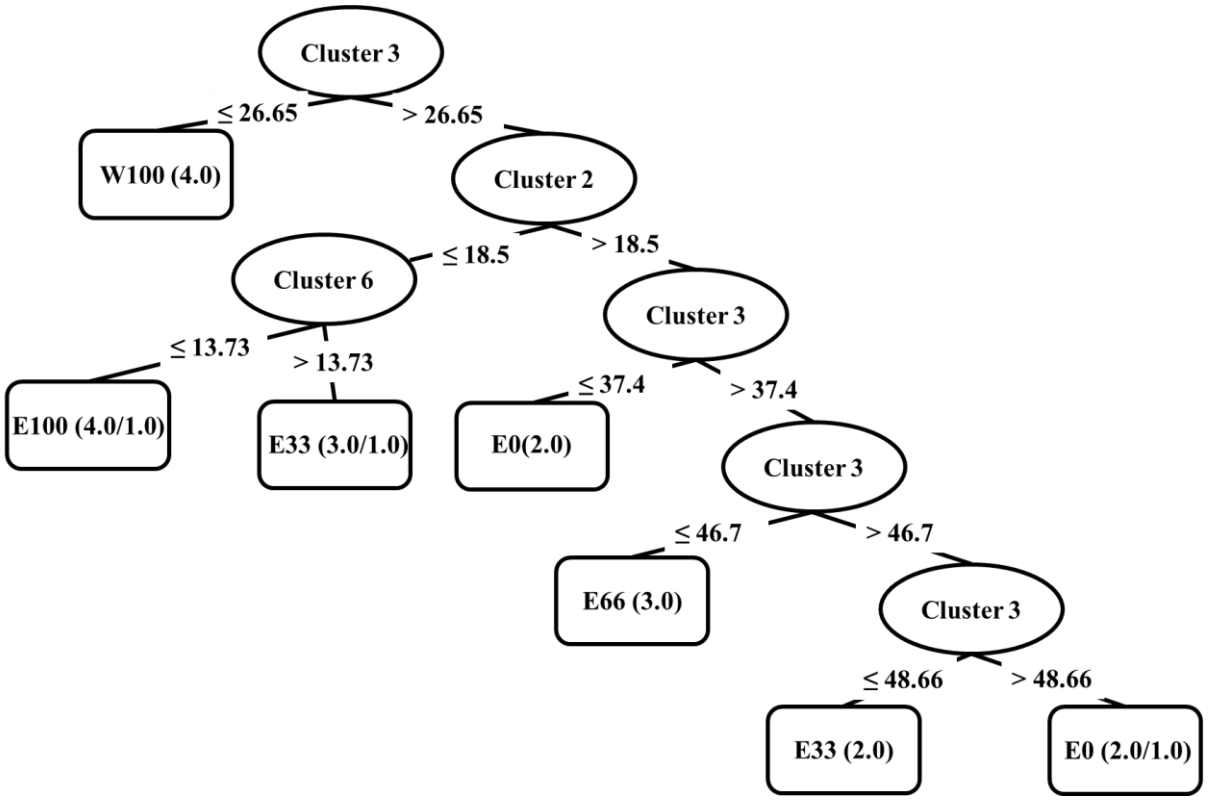

Figure 20. Ninth aerial evaluation. Decision tree that explored the paths that recognized the wastewater treatments. Source: Own author

Table 10. Ninth aerial evaluation. Confusion matrix evaluating the classifier.

Confusion Matrix		Predicted Class				
		E0	E33	E66	E100	W100
Actual Class	E0	3	0	0	1	0
	E33	0	4	0	0	0
	E66	1	0	3	0	0
	E100	0	1	0	3	0
	W100	0	0	0	0	4

Source: Own author.

Table 11. Ninth aerial evaluation. Decision tree outputs about the size and complexity of the system.

Aerial Evaluation	Color Space	First Decision Tree			Second Decision Tree		
		Accuracy	Leaves	Nodes	Accuracy	Leaves	Nodes
Time 08	Hue	85%	7	13	100%	10	19

Source: Own author.

Table 12. Ninth aerial evaluation. Paths that led to leaves of decision tree transformed into a set of rules.

If Cluster3 <= 26.65 then W100
If Cluster3 > 26.65 and Cluster2 <= 18.5 and Cluster6 <= 13.73 then E100
If Cluster3 > 26.65 and Cluster2 <= 18.5 and Cluster6 > 13.73 then E33
If Cluster3 > 26.65 and Cluster2 > 18.5 and Cluster3 <= 37.4 then E0
If Cluster3 > 26.65 and Cluster2 > 18.5 and Cluster3 >37.4 and Cluster3 <= 46.7 then E66
If Cluster3 > 26.65 and Cluster2 > 18.5 and Cluster3 >37.4 and Cluster3 > 46.7 and Cluster3 <= 48.66 then E33
If Cluster3 > 26.65 and Cluster2 > 18.5 and Cluster3 >37.4 and Cluster3 > 46.7 and Cluster3 > 48.66 then E0

Source: Own author.

5. **CONCLUSIONS**

The cybernetic cohesion information flow was achieved with success because no discontinuance in the process of information extraction of an agricultura crop was found. But some improvements could be done in further researches such as another's platforms of python software (anaconda, jupyter and spyder) and embody of Arduino open source program for eletronic devides

In this work we conclude that the time required for construction of georeferenced orthomosaic is directly related to the number of images processed in Agisoft PhotoScan Professional software. The most expensive step in time and processor memory was the construction of dense point cloud (3D model).

We have succeeded in integrating the platforms Quantum Gis, Python and Weka. Their power to analyze the RGB spectral information was evident.

The computational algorithms used allowed delimitation of the parcels, transformation from the RGB to HSV color space, grouping by the K-means method, classification by the decision tree and usage of set theory and algebraic map.

The integration of precision agriculture and artificial intelligence has been achieved within the proposed because the errors were minimal within the geographical positioning and computational algorithms have reached maximum success rate.

.

REFERENCES:

AI, L. et al. Broad area mapping of monthly soil erosion risk using fuzzy decision tree approach: integration of multi-source data within GIS. International Journal of Geographical Information Science, v. 27, n. 6, p. 1251-1267, Jun 2013.

AGUERA-VEGA, F.; CARVAJAL-RAMIREZ, F.; MARTINEZ-CARRICONDO, P. Assessment of photogrammetric mapping accuracy based on variation ground control points number using unmanned aerial vehicle. Measurement, v. 98, p. 221-227, Feb 2017. ISSN 0263-2241. Disponível em: < <Go to ISI>://WOS:000393241200024 >.

AL-ABADI, A. M. et al. A GIS-Based Integrated Fuzzy Logic and Analytic Hierarchy Process Model for Assessing Water-Harvesting Zones in Northeastern Maysan Governorate, Iraq. Arabian Journal for Science and Engineering, v. 42, n. 6, p. 2487-2499, Jun 2017.

ALPAYDIN, E. Introduction to Machine Learning (second ed.), The MIT Press Cambridge, Massachusetts, London, England (2010)

BISHOP, C. Pattern Recognition and Machine Learning. Springer (2006)

BUI, D. T. et al. A hybrid artificial intelligence approach using GIS-based neural-fuzzy inference system and particle swarm optimization for forest fire susceptibility modeling at a tropical area. Agricultural and Forest Meteorology, v. 233, p. 32-44, Feb 2017.

BURROUGH P. A., MCDONNELL R. A., LLOYD C. D. Principles of Geographical Information Systems. (3rd edition), 352 p. Oxford University Press, 2015.

CANTOR, G. Grundlagen Einer Allgemeinen Mannigfaltigkeitslehre, Teubner, Leipzig, 1883.

CHIABRANDO, F.; DONADIO, E.; RINAUDO, F. SfM for orthophoto generation: a winning approach for cultural heritage knowledge. 25th International Cipa Symposium 2015, v. 40-5, n. W7, p. 91-98, 2015. ISSN 2194-9034. Disponível em: < <Go to ISI>://WOS:000380437800014 >.

DUAN, T. et al. Dynamic monitoring of NDVI in wheat agronomy and breeding trials using an unmanned aerial vehicle. Field Crops Research, v. 210, p. 71-80, Aug 2017

FORSYTH, D. A.; PONCE, J. Computer Vision: A Modern Approach. Prentice-Hall (2003)

GREWAL, M.; ANDREWS, A.P.; BARTONE, C.G. Global navigation satellite systems, inertial navigation, and integration (3rd edition), John Wiley & Sons, Inc., Hoboken, New Jersey (2013)

HALMOS, P. Naive Set Theory. Princeton, NJ: D. Van Nostrand Company, 1960. Reprinted by Springer-Verlag, New York, 1974

HAMUDA, E. et al. Automatic crop detection under field conditions using the HSV colour space and morphological operations. Computers and Electronics in Agriculture, v. 133, p. 97-107, Feb 2017.

LIU, J. G.; MOORE, J. M. Hue image RGB color composition - a simple technique to suppress shadow and enhance spectral signature. International Journal of Remote Sensing, v. 11, n. 8, p. 1521-1530, Aug 1990.

LLOYD, S. P. (1982). Least squares quantization in PCM. IEEE Transactions on Information Theory, 28, 129–137.

MADDAHI, Z. et al. Land Suitability Analysis for Rice Cultivation Using a GIS-based Fuzzy Multi-criteria Decision Making Approach: Central Part of Amol District, Iran. Soil and Water Research, v. 12, n. 1, p. 29-38, 2017.

MENDOZA, F.; LU, R. 2015. Basics of image analysis. In: Park, B., Lu, R., editors. Hyperspectral Imaging Technology In Food and Agriculture. New York, NY: Springer.

MENG, Q. K. et al. Development of agricultural implement system based on machine vision and fuzzy control. Computers and Electronics in Agriculture, v. 112, p. 128-138, Mar 2015. ISSN 0168-1699. Disponível em: < <Go to ISI>://WOS:000353845600017 >.

MOLIN, J.P.; AMARAL L.R.; COLAÇO A.F. Agricultura de Precisão. São Paulo: Oficina de Textos, 2015

OPENSHAW, S. Some suggestions concerning the development of artificial-intelligence tools for spatial modeling and analysis in gis. Annals of Regional Science, v. 26, n. 1, p. 35-51, Apr 1992

PEDRYCZ, W.; GOMIDE, F. Fuzzy Systems Engineering, John Wiley & Sons, Hoboken, NJ, USA, 2007.

RUIZ-RUIZ, G.; GOMEZ-GIL, J.; NAVAS-GRACIA, L. M. Testing different color spaces based on hue for the environmentally adaptive segmentation algorithm (EASA). Computers and Electronics in Agriculture, v. 68, n. 1, p. 88-96, Aug 2009.

SILVA, I.N.; SPATTI D.; FLAUZINO, R. Redes neurais artificiais para engenharia e ciências aplicadas: curso prático, Artliber Editora Ltda, São Paulo, SP, Brasil. 2010. ISBN978-85-88098-53-4

SZELISKI, R.: Computer Vision: Algorithms and Applications. Springer, London (2011)

WEISS, M.; BARET, F. Using 3D Point Clouds Derived from UAV RGB Imagery to Describe Vineyard 3D Macro- Structure. Remote Sensing, v. 9, n. 2, p. 17, Feb 2017. ISSN 2072-4292. Disponível em: < <Go to ISI>://WOS:000397013700013 >.

YANG, W. et al. Greenness identification based on HSV decision tree. Information Processing in Agriculture, v. 2, n. 3, p. 149-160, 2015/10/01/ 2015. ISSN 2214-3173. Disponível em: < http://www.sciencedirect.com/science/article/pii/S2214317315000347 >.

ZHANG, C. H.; KOVACS, J. M. The application of small unmanned aerial systems for precision agriculture: a review. Precision Agriculture, v. 13, n. 6, p. 693-712, Dec 2012. ISSN 1385-2256. Disponível em: < <Go to ISI>://WOS:000310746000006 >.

ZAKI M.J.; MEIRA W. Jr. Data mining and analysis fundamental concepts and algorithms. New York: Cambridge University Press; 2014.